Absolute silicon photodiodes for 160 nm to 254 nm photons

L. R. Canfield, R. E. Vest, R. Korde, H. Schmidtke and R. Desor

Abstract. Silicon n-on-p photodiodes with 100 % internal quantum efficiency have been studied in the 160 nm to 254 nm spectral range. Preliminary values have been determined for the quantum yield of silicon at these wavelengths. Using these values, a trap detector is presented for absolute flux measurement in this region. The stability under intense 193 nm irradiation, a property of importance in lithography and in photorefractive keratectomy, has been measured, and the diodes tested were found to be several orders of magnitude more stable than p-on-n diodes tested by other investigators at this wavelength. Spatial nonuniformities of the n-on-p diodes were found to be less than 1 % at wavelengths of 254 nm and 161 nm.

1. Introduction

For decades, silicon photodiodes have been widely used in the visible/near-infrared radiometry community. Designs which exhibit excellent spatial uniformity and stability are frequently used as calibrated transfer standards, or as the components of absolute devices such as trap detectors. However, it has been recognized that as spectral coverage is extended into the ultraviolet, photodiodes that were satisfactory in the visible/near-infrared spectral region exhibit significant problems. The advent of lithography systems and medical applications based on KrF (248 nm) and ArF (193 nm) lasers makes the development of improved detectors extremely important.

We report a study, over the spectral region 160 nm to 254 nm, of silicon photodiodes which have been shown [1] to have properties enabling them to be used as transfer standards for the extreme ultraviolet. These photodiodes have an n-on-p construction with a nitrided passivating SiO_2 surface layer. A schematic of the general construction of the 1 cm^2 active-area photodiode investigated is shown in Figure 1.

All experimental measurements in this study were conducted without bias on the photodiodes. Uniformity measurements at 254 nm were conducted at International Radiation Detectors, and stability measurements at 193 nm were conducted at Lambda Physik Lasertechnik. The other measurements were made at the National Institute of Standards and Technology (NIST).

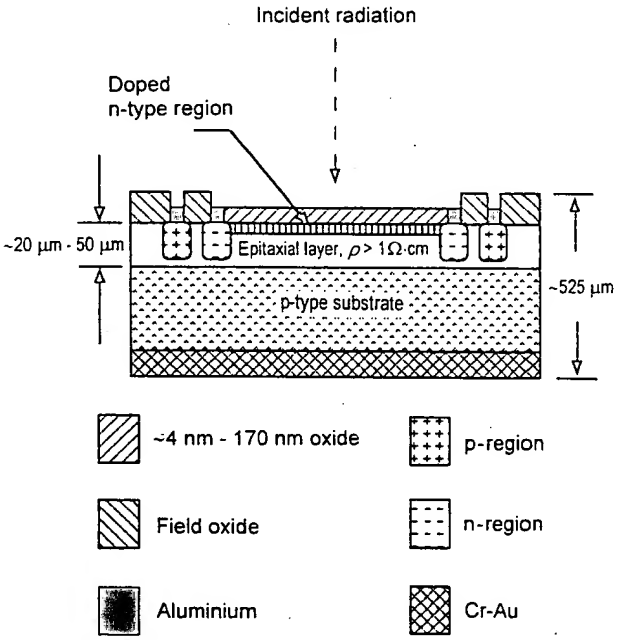

Figure 1. Schematic of the silicon photodiodes.

2. Quantum yield

The quantum yield (the number of electron-hole pairs produced per photon transmitted into the silicon) of these photodiodes in the 160 nm to 254 nm wavelength range can be deduced from a determination of reflective

L. R. Canfield and R. E. Vest: Electron and Optical Physics Division, Physics Laboratory, National Institute of Standards and Technology, Technology Administration, US Department of Commerce, Gaithersburg, MD 20899-0001, USA.
R. Korde: International Radiation Detectors, Torrance, CA 90505-5229, USA.
H. Schmidtke and R. Desor: Lambda Physik Lasertechnik, D-37079 Göttingen, Germany.

losses and measurement of the external quantum efficiency (the number of electron-hole pairs produced per photon incident on the device). The photodiodes are essentially free of internal losses (recombination in the doped n-region or at the surface) [2], and the passivating silicon-dioxide surface film has negligible absorption in this region, so only knowledge of the external efficiency and the reflectance of the oxide layer is required to obtain the quantum yield.

The external efficiency as a function of wavelength of each photodiode was measured by alternately exposing the sample photodiode and a NIST-calibrated working standard photodiode to the same monochromatic radiation, and measuring the photocurrent from each. The working standard photodiode traces to both a rare gas ionization chamber [3] and the calculable irradiance from the NIST Synchrotron Ultraviolet Radiation Facility (SURF II) electron storage ring [4]. The reflective loss as a function of wavelength was determined by Fresnel calculations, based on published optical constants [5], using oxide thicknesses measured with an ellipsometer. (The photodiodes are basically a non-absorbing film on an opaque substrate.) The thickness measurements were confirmed by comparing the spectral location of interference features from these calculations with similar features in the measured external efficiency data. Figure 2 shows the measured external efficiency of a representative photodiode and the calculated transmittance into silicon for the thickness of oxide measured.

Nine photodiodes, selected from different wafers and with oxide thicknesses ranging from 4 nm to 170 nm, were used in this study. The quantum yield of each sample was calculated from the simple relationship

$$Y(\lambda) = \frac{i_{\mathrm{samp}}(\lambda)}{i_{\mathrm{std}}(\lambda)} \cdot \frac{\varepsilon_{\mathrm{std}}(\lambda)}{T(\lambda)}, \qquad (1)$$

where Y is the quantum yield, i_{samp} and i_{std} are the measured photocurrents of the sample and standard, respectively, $\varepsilon_{\mathrm{std}}$ is the external quantum efficiency of the standard, and T is the calculated transmittance into the silicon, each quantity being a function of wavelength λ. It is assumed that there are no internal losses and that the published optical constants for amorphous silicon dioxide and crystalline silicon are appropriate for the Fresnel calculations.

The quantum yield in the 160 nm to 254 nm spectral region, as determined by the above method, is plotted in Figure 3, which shows the spread in the values found from the nine photodiodes, and the average of these measurements. Note that not only did these photodiodes have a wide range of oxide thicknesses, but they were selected from wafers manufactured at four different times. Also shown in Figure 3 are previously published [2] values of the quantum yield at somewhat longer wavelengths. The value of 1.21 pair/photon obtained at 254 nm is also in reasonable agreement with the value of 1.13 pair/photon given in a 1993 publication [6].

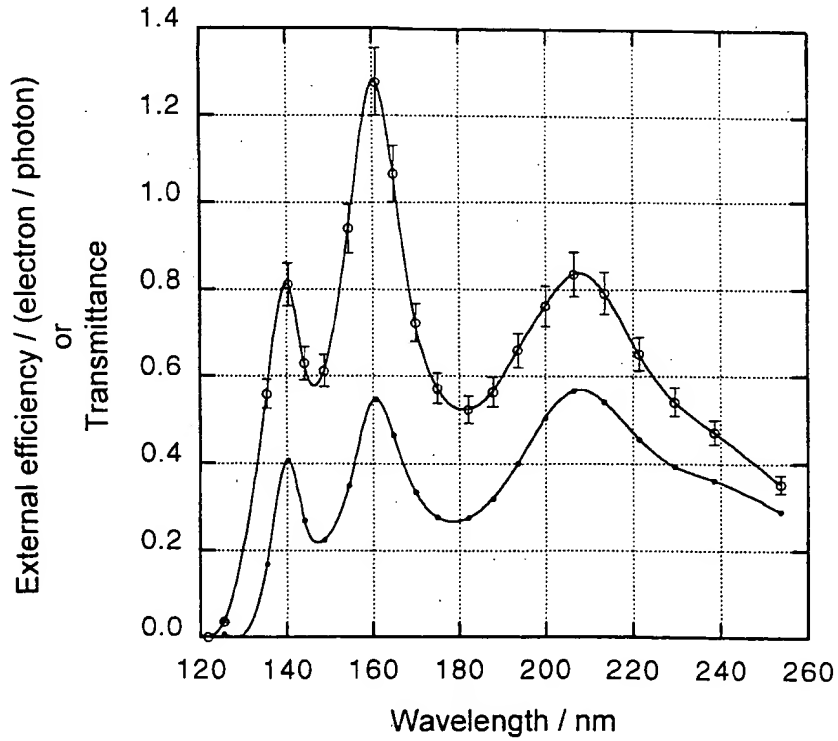

Figure 2. Calculated (•) normal incidence transmittance into silicon of a photodiode with 159 nm oxide thickness, compared with the measured (o) external efficiency of a photodiode with this oxide thickness. The combined standard uncertainties are shown for the measured data. Both sets of data are fitted with cubic splines.

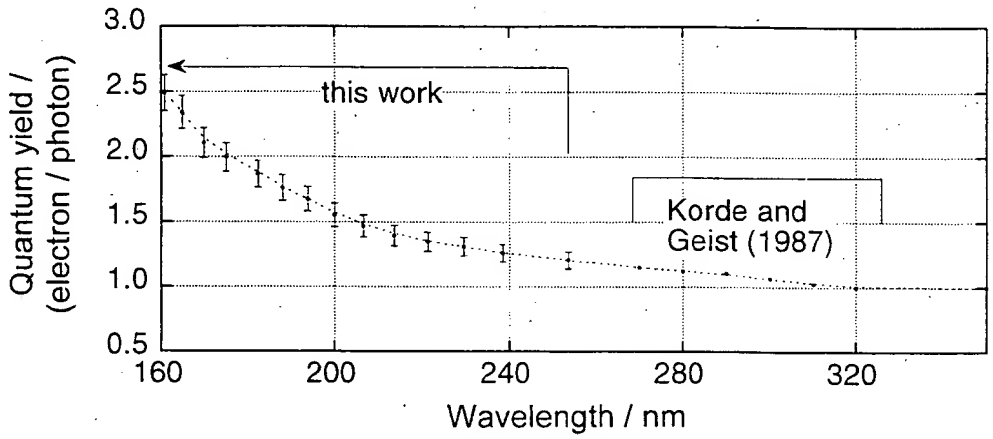

Figure 3. The quantum yield of silicon from 160 nm to 254 nm, determined in this study. Also shown from 270 nm to 350 nm are the results given in [2], with a smooth curve joining all data points. The combined standard uncertainty is shown for each of the present values; this includes the statistical variation of the measurements on the group of nine photodiodes, and the estimated uncertainties of the quantum efficiency and transmittance terms of (1), all summed in quadrature.

The measured pair creation energy, which is about 3.10 eV/pair at 160 nm, is significantly lower than the generally accepted high-energy value of about 3.6 eV/pair, and appears to decrease with increasing photon energy (decreasing wavelength). This does not necessarily indicate a problem with the measured results. The theory of the quantum yield in this spectral region predicts features associated with transitions from the band edges that can give rise to pair creation energies well below the high-energy value [7, 8]. An extension of the existing calculations to higher energies is needed to determine whether the high quantum yields reported here are consistent with current quantum-yield theory.

The variations in the quantum yields determined from a group (B) of photodiodes from a single wafer, with the as-grown oxide thicknesses chemically thinned, are only slightly less than those from the entire group (A). Table 1 gives the standard deviation of the quantum yield determined from each group at a few selected wavelengths in the region studied. The table shows that there is minimal dependence on sample identity.

Table 1. Relative standard deviations (σ) of the silicon quantum yields determined from two groups of photodiodes. Group A contains nine chips from four different wafers, while group B comprises five chips from one of the group A wafers, but with a variety of oxide thicknesses (obtained by thinning the as-grown thickness). λ is the incident photon wavelength.

	$100 \times \sigma$	
λ / nm	Group A	Group B
160.8	4.2	4.1
175.0	2.9	2.9
200.0	5.9	3.4
229.6	3.0	2.4

Continuation of quantum-yield measurements to even shorter wavelengths revealed that the results in this region are not independent of oxide thickness. There is progressively greater absorption in the oxide as the wavelength decreases below about 160 nm, with the extinction coefficient reaching a maximum just short of 120 nm. It has also been observed [9-11] that at short wavelengths there appears to be charge transport from the oxide into the silicon, so the determination of quantum yield becomes much more complex.

Although these results are important (the quantum yield of silicon has been measured for the first time in the 160 nm to 254 nm spectral region, with an estimated relative combined standard uncertainty of 6 %; see Figure 3), the quantum yield of silicon in this region could be determined with much lower uncertainty using other techniques. Measurement of the external quantum efficiency of photodiodes using a cryogenic radiometer should greatly reduce the uncertainty obtained here, and direct measurement of the reflectivity of each device would eliminate any dependence on optical-constants data. Using this approach it should be possible to achieve quantum-yield measurements with relative combined standard uncertainties of about 1%. Preliminary measurements of this type have been conducted with the new NIST cryogenic radiometer facility at the SURF II electron storage ring. These results are in general agreement with those given here, and will be reported in a subsequent publication [12].

3. Spatial uniformity

To determine the spatial uniformity of the response, scans were made of randomly chosen photodiodes at wavelengths of 160.8 nm and 253.7 nm. The procedure at 160.8 nm was to scan the detector behind a fixed aperture placed in the path of radiation emerging from the exit slit of a vacuum monochromator with a hydrogen plasma source. The bandwidth of the radiation

was approximately 0.3 nm, and the beam diameter on the detector was approximately 0.5 mm. The 253.7 nm scan was done using a low-pressure Hg source and a beam diameter of approximately 1 mm. The results of these scans are shown in Figures 4 and 5, respectively.

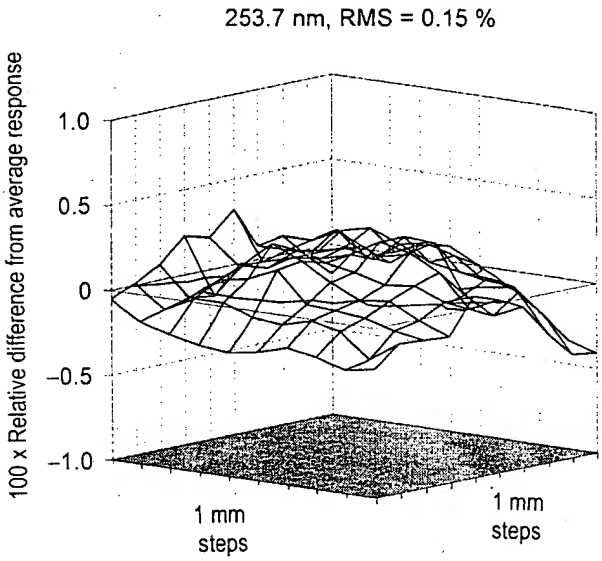

Figure 4. Spatial variation from the average response of one of the studied photodiodes at $\lambda = 253.7$ nm.

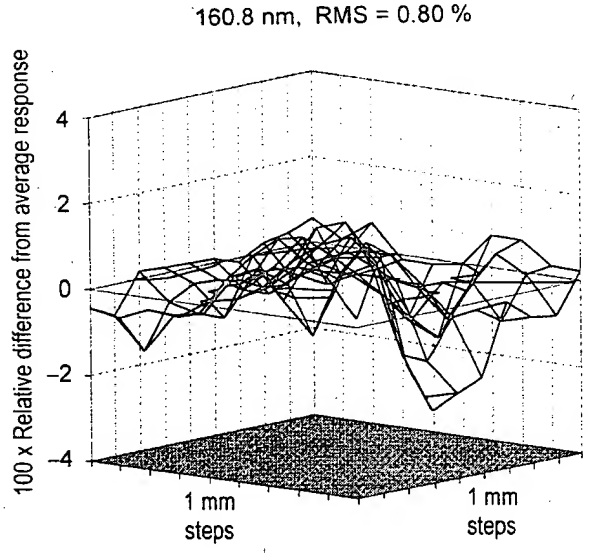

Figure 5. Spatial variation from the average response of one of the studied photodiodes at $\lambda = 160.8$ nm.

4. Responsivity stability

A representative n-on-p photodiode was illuminated with intense 193 nm radiation from a pulsed ArF laser to study the stability of response at this wavelength. Lasers of this type are increasingly being used for lithography and in certain medical procedures. The pulse rate was 100 Hz, and the laser was operated in a constant-energy mode. The beam from the laser was masked to ensure that the photodiode was underfilled, and was attenuated to give an energy density of approximately 200 mJ/cm^2 at the detector. Photocurrent pulses produced by the radiation were integrated by an oscilloscope, and recorded as a function of time (and therefore exposure). The output power of the laser was checked at the beginning and end of the test with a commercial power meter. The effect of such an exposure on a silicon photodiode of the type studied here is shown in Figure 6. Also shown in this figure is the effect [13] of a similar exposure on a commercial p-on-n silicon photodiode of a type commonly chosen for its stability in the visible and near-ultraviolet spectral regions. Both curves are normalized to the initial response.

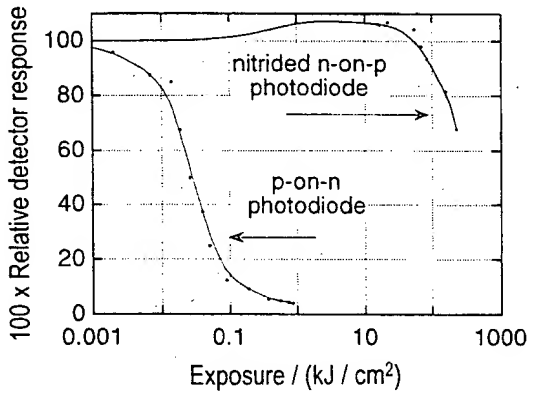

Figure 6. The degradation of one of the n-on-p silicon photodiodes during prolonged exposure to a pulsed laser at $\lambda = 193$ nm. Also plotted is the corresponding degradation of a p-on-n silicon photodiode.

5. An absolute detector for 160 nm to 254 nm

Knowledge of the quantum yield of silicon and production of stable photodiodes should allow the use of trap detectors in this spectral region. Traps with a variety of configurations have been the subject of several previous publications (see, for example, [14] and [15]), but detectors of this type have not been reported for the region studied here. Traps are commonly used in regions where the quantum yield of silicon is known to be unity, and where the reflective loss from the detector surfaces is not great. There appears to be no reason why one cannot design silicon photodiode traps for all portions of the spectral region in which silicon photodiodes operate, if the quantum yield of silicon is known and there are no internal losses in either the oxide or the silicon. One may need to allow for large reflective losses, as are found in the region studied here, by allowing a large number of detection/reflection events within the active length chosen.

There are a number of designs that might be used for a trap for the 160 nm to 254 nm region. We limit this

discussion to a single configuration, and do not address all the specific secondary design considerations, such as polarization sensitivity, scatter, etc. It should also be noted that the present state of detector radiometry in this spectral region, particularly in the vacuum portion, means that the low calibration uncertainties typical in the visible/near-infrared region cannot be matched.

For this exercise, we have selected a convergent trap design similar to one described in [15]. Rather than a number of discrete photodiodes, our implementation uses two photodiodes electrically connected in parallel and arranged so that multiple reflections (and detection events) occur on each detector. The key elements to making such a detector feasible are knowledge of the silicon quantum yield and the use of photodiodes with negligible internal losses. We presume the application in our example to be the monitoring of 193 nm radiation, as in lithography.

A trap detector of any configuration will obviously absorb incident radiation most efficiently if the reflectivity of the detecting elements is minimized. Figure 7 is a plot of the calculated reflectance for normal incidence of radiation of $\lambda = 193$ nm on a silicon photodiode, as a function of surface oxide thickness. We can explore the performance by starting with a best-case match, in which the reflectance would be about 0.45. In any trap detector there will be some unabsorbed (and therefore undetected) radiation that escapes from the trap, usually after many reflections. Our goal is to limit the fraction of unabsorbed radiation to 0.005 and we arbitrarily limit the active length of each photodiode to 3 cm (an available length for the photodiodes discussed here).

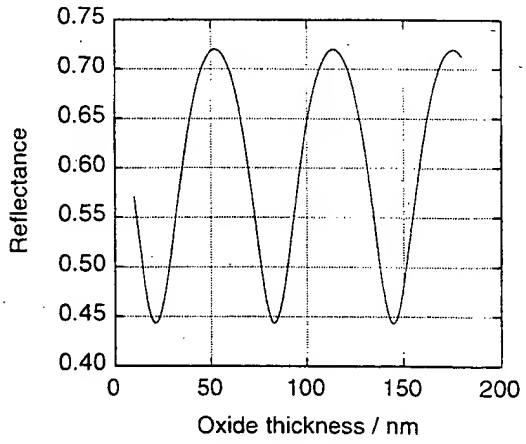

Figure 7. Calculated normal incidence reflectance of a silicon photodiode as a function of passivating oxide thickness at a wavelength of 193 nm.

The general mechanical configuration for this trap is shown in Figure 8. In the figure, Δ is the angle of convergence of the left detector relative to the right, while Θ is the initial angle of incidence of the radiation. It is clear that the angle of incidence on the photodiode is not the same for each reflection. It is, however, never

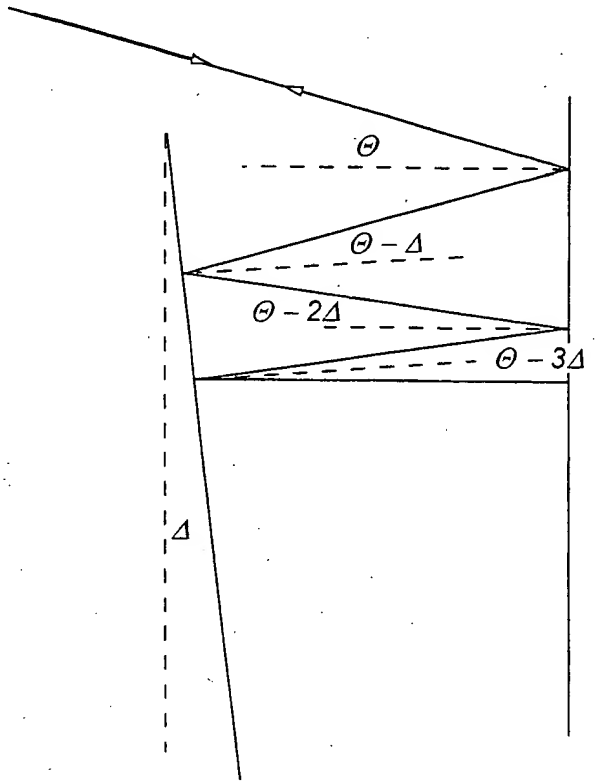

Figure 8. One possible design for a trap detector for use in the 160 nm to 254 nm region, using two silicon photodiodes of the type studied.

larger than Θ, which is near normal incidence, and the actual reflectance will not be very much different than the normal incidence reflectance. This variation in the actual angle of incidence complicates the analysis, but we can use the normal incidence value to demonstrate the feasibility of a trap detector in the 160 nm to 254 nm spectral region.

If we arbitrarily fix Θ at 14° with the detectors separated by 10 mm, and then adjust Δ to meet or exceed the unabsorbed radiation goal, we find that an angle of 4° will result in an undetected fraction of 0.0037. There will be a total (including reversal) of seven reflections, and the detector length required will be 6.7 mm from the point of first incidence. If we move to a worst-case oxide thickness, the reflectance would be about 0.72, and $\Delta = 1.6°$ will be required to achieve the target of 0.005. With this angle, there will be a total of seventeen reflections, giving an undetected fraction of 0.0038 in 13.8 mm of travel. This would simulate the operation of the trap at neighbouring wavelengths, for which it was not optimized. It might be advantageous, in general, to make the angle Δ easily adjustable to accommodate various oxide thicknesses on the photodiodes, to facilitate optimized use at more than one wavelength, and perhaps to allow the use of either end of the assembly as the entrance/exit.

The angular spread of incident radiation that would be accepted by such a trap would be of concern to many applications. For the optimized case above, with

the reflectance equal to 0.45, but with $\Delta = 1.6°$, the detector would accept $\pm 6°$ within the chosen length of 3.0 cm. The undetected component would be well below the target for any incidence angle within the specified range.

6. Conclusions

The quantum yield of silicon in the 160 nm to 254 nm region has been determined for the first time. Knowledge of this quantum yield allows the development of trap detectors to be used as absolute devices. These absolute trap detectors will be extremely useful for determinations of excimer laser doses during deep-ultraviolet lithography and photorefractive and phototherapeutic keratectomy, as present detectors used in these applications are not satisfactory. Theoretical models need to be developed to explain the observed quantum yield.

Acknowledgement. This work was supported in part by grant No. 5 R44 GM47180-03, from the US National Institutes of Health.

References

1. Gullikson E. M., Korde R., Canfield L. R., Vest R. E., *J. Elect. Spectr. Rel. Phenom.*, 1996, **80**, 313-316.
2. Korde R., Geist J., *Appl. Opt.*, 1987, **26**, 5284-5290.
3. Samson J. A. R., Haddad G. N., *J. Opt. Soc. Am.*, 1974, **64**, 47-54.
4. Vest R. E., Canfield L. R., Furst M. L., Madden R. P., Swanson N., *Nucl. Instrum. Methods*, 1994, **A347**, 291-293.
5. Palik E. D., *Handbook of Optical Constants of Solids*, New York, Academic Press, 1985.
6. Durant N. M., Fox N. P., *Metrologia*, 1993, **30**, 345-350.
7. Geist J., Wang C. S., *Phys. Rev.*, 1983, **B27**, 4841-4847.
8. Kolodinski S., Werner J. H., Wittchen T., Queisser H. J., *Appl. Phys. Lett.*, 1993, **63**, 2405-2407.
9. Saito T., Hughey L. R., Proctor J. E., O'Brian T. R., *Rev. Sci. Instrum.*, 1996, **67**, on CD-ROM.
10. Canfield L. R., Kerner J., Korde R., *Appl. Opt.*, 1989, **28**, 3940-3943.
11. Funsten H. O., Suszcynsky D. M., Ritzau S. M., Korde R., *1996 IEEE Nuclear Science Symposium Conference Record*, 608-613.
12. Lykke K., Shaw P.-S., Gupta R., personal communication.
13. Product brochure, UVC TECHnology, Hamburg, Germany, 1997.
14. Zalewski E. F., Duda C. R., *Appl. Opt.*, 1983, **22**, 2867-2873.
15. Palmer J. M., *Metrologia*, 1993, **30**, 327-333.